water

MDPI

Article

Backward Trajectory Analysis Based on Specific Humidity Correction for the Influence of Moisture Sources on Precipitation Isotopes in the Western Loess Plateau, China

Xiaobo Yue [1,2], Mingjun Zhang [1,2,*], Deye Qu [1,2], Shengjie Wang [1,2], Fenli Chen [1,2], Yu Zhang [1,2] and Yuanyuan Tian [1,2]

[1] College of Geography and Environmental Science, Northwest Normal University, Lanzhou 730070, China
[2] Key Laboratory of Resource Environment and Sustainable Development of Oasis, Lanzhou 730070, China
* Correspondence: mjzhang2004@163.com

Abstract: Based on the precipitation samples collected in Minxian in the western Loess Plateau from 2019 to 2021, this study analyzes the influence of moisture sources on precipitation isotopes. Through the specific humidity correction of the backward trajectory, it is found that Xinjiang and the middle and lower reaches of the Yangtze River may be the main moisture sources. Through cluster analysis of backward trajectories, it is found that in the summer half-year, the water vapor from the east and northeast leads to the precipitation with a depleted isotope ratio, while the water vapor from the south and northwest leads to the precipitation with an enriched isotope ratio; in the winter half, water vapor from the east leads to precipitation with enriched isotope ratios, while water vapor from the northwest and northeast leads to precipitation with depleted isotope ratios. In addition, the precipitation isotope values showed a tendency to deplete with the duration of water vapor transport in the summer half-year, but this tendency was not obvious in the winter half-year. The relationship between precipitation isotopes and water vapor transport height showed a positive correlation in both the winter half-year and summer half-year. Using the Potential Source Contribution Factor analysis methods and the backward trajectory after the specific humidity revision, it was found that the potential evaporation source areas in the summer half-year are larger in extent, mainly distributed in the eastern and southern regions of the sampling site, and the contribution of local recycled vapor to precipitation is 32.17%; while the potential evaporation source areas in the winter half-year are smaller in extent, they are only distributed in the southern region of the sampling site, and the contribution of local recycled vapor to precipitation is 24.66%.

Keywords: moisture source; specific humidity correction; potential evaporation source areas; local recycled vapor

check for updates

Citation: Yue, X.; Zhang, M.; Qu, D.; Wang, S.; Chen, F.; Zhang, Y.; Tian, Y. Backward Trajectory Analysis Based on Specific Humidity Correction for the Influence of Moisture Sources on Precipitation Isotopes in the Western Loess Plateau, China. *Water* **2022**, *14*, 3452. https://doi.org/10.3390/w14213452

Academic Editor: Jun Asanuma

Received: 24 September 2022
Accepted: 27 October 2022
Published: 29 October 2022

1. Introduction

As one of the most important links in the water cycle, precipitation plays a key role in providing water resources and ecosystem services for human development [1,2]. Hydrogen- and oxygen-stable isotopes are important components of water molecules and have been considered as ideal tracers in past studies, often used in the study of water cycle processes and paleoclimate reconstructions [3–5]. In the context of global warming, water cycle processes are changing [6–8]. Therefore, the study of the spatial and temporal characteristics of precipitation isotope changes and the influencing factors will not only help us to deeply understand the regional water cycle processes but also provide a unique perspective for the reconstruction of the paleoclimate and the study of hot issues such as global climate change.

The study of precipitation isotopes began in the 1960s, and the initial studies concluded that the fluctuations of precipitation isotopes are mainly related to local meteorological factors and geographical parameters, and these relationships are called environmental

effects of precipitation isotopes and present different combinations in different geographical contexts [9–11]. However, precipitation is the transport of evaporated water vapor from the moisture source area, which condenses and rises to cool under a specific form of atmospheric circulation, which in turn produces precipitation cover [12]. In this process, precipitation isotopes are influenced by many factors; the difference in moisture sources is the initial cause of precipitation isotope differences, and subsequent processes are based on which precipitation isotopes are modified [13–16]. Therefore, studying the influence of moisture sources on precipitation isotopes will help us to understand the variation of precipitation isotopes.

D-excess (*d-excess* = δ^2H-8δ^{18}O), as a secondary variable of precipitation isotopes, can effectively eliminate covariates of hydrogen and oxygen isotopic composition, which is influenced by the relative humidity and sea surface temperature in the moisture source region and is usually used for moisture source identification [17,18]. However, subcloud evaporation and local water vapor recirculation processes can produce variations in *d-excess*, which can introduce errors in its indication of moisture sources [19,20]. Subsequent researchers have developed a series of models for moisture source studies, with backward trajectory models being the most widely used [21–23]. Numerous studies have shown that precipitation vapor is not only exogenously transported water vapor but also local recycled vapor produced by surface evaporation, and plant transpiration is an important component of precipitation vapor [24,25]. The backward trajectory model can clearly simulate the exogenous transported water vapor but it cannot assess the contribution of local recycled vapor to precipitation. Two-component mixing models and three-component mixing models with nested isotopes are often used to calculate the contribution of local recycled vapor to precipitation [26–29], which has facilitated research in the area of moisture sources.

Minxian is located in the transition area between the Loess Plateau and Tibetan Plateau in China, which is influenced by both the East Asian monsoon and westerlies, and the special geographical location makes the moisture sources in this area very complex. Moisture sources and their effects on precipitation isotopes have been studied by previous authors using backward trajectory models, two-component mixing models and three-component mixing models [29–33]. However, when these studies applied backward trajectory models to study the external transported water vapor, the meteorological elements on the backward trajectory were not taken into account; and when two-component mixing models and three-component mixing models were used to study the local recycled vapor, the settings and inputs of many parameters in the models were inferred from empirical equations and substitutions, and two-component mixing models and three-component mixing models were unable to simulate the spatial extent of the generation of local recycled vapor, which limited the study of moisture sources and their effects on precipitation isotopes. Therefore, this paper will use the data collected in Minxian to study the influence of moisture sources on precipitation isotopes by improving the backward trajectory model. The objectives of this research are to (1) further clarify the moisture source area of precipitation in the study area by performing the specific humidity correction of the backward trajectory; (2) study the effects of moisture source area, water vapor transport time, and water vapor transport height on precipitation isotopes based on the backward trajectory after the specific humidity correction; (3) using the PSCF model, to identify potential evaporation source areas affecting precipitation in the study area and combine this with backward trajectories corrected by specific humidity to assess the contribution of local recycled vapor to precipitation. This study will deepen the understanding of water circulation processes in the western part of the Loess Plateau and provide meaningful references for the reconstruction of the paleoclimate.

2. Data and Method

2.1. Study Area

All samples of this study were collected in Minxian, south of Dingxi City, Gansu Province, China, which is located in the western part of the Loess Plateau and the eastern

foot of the Tibetan Plateau, with the surrounding terrain being mostly mountainous and hilly and with high vegetation cover (Figure 1). The climate of the area is temperate and semi-humid, and according to historical meteorological data from 1961 to 2020 (Figure 2), its multi-year average temperature is 6.06 °C, multi-year average relative humidity is 67.72%, and multi-year average precipitation is 582.43 mm. Based on the threshold of 10% of the multi-year average precipitation, the sampling site can be divided into the summer half of the year from May to September, and the winter half of the year from October to April [34]. During the summer half-year, the average temperature of the area is 13.90 °C, concentrating more than 75% of the precipitation throughout the year, and the climate is relatively warm and humid, while during the winter half-year, the prevailing westerly winds and southward continental air masses cause the area to be cold and dry with an average temperature of 0.45 °C.

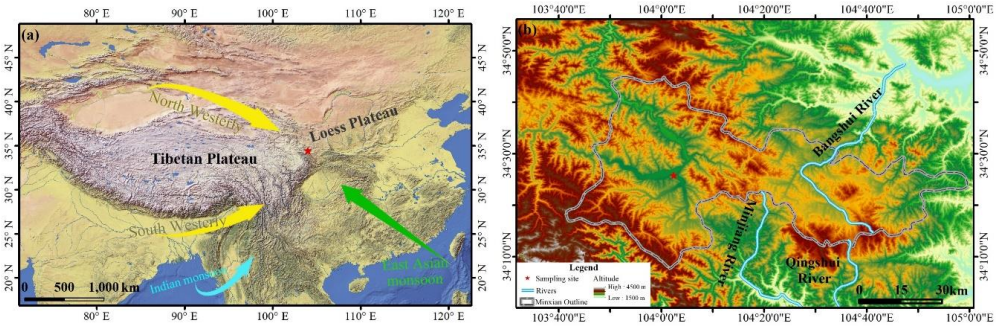

Figure 1. Map showing the location of Minxian (**a**) in the Loess Plateau (**b**).

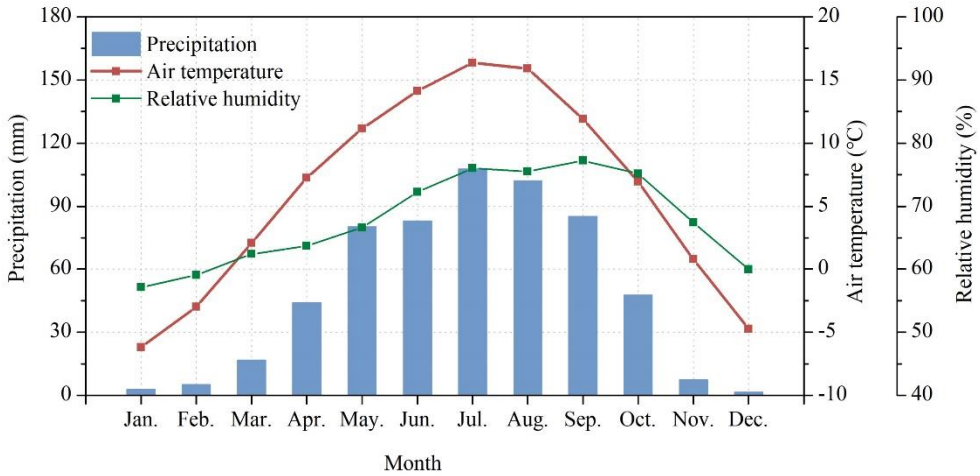

Figure 2. Multi-year averages of seasonal patterns of precipitation, air temperature and relative humidity in Minxian (1961–2020).

2.2. Precipitation Sample Collection

In this study, 188 precipitation event samples collected in Minxian during two time periods from April 2019 to October 2021 were used, with 89 precipitation event samples collected in the first stage from May 2019 to May 2020 and 89 precipitation event samples collected in the second stage from September 2020 to October 2021. All precipitation samples were collected by full-time meteorological observers from the local meteorological office, and the sampler was a standard 20cm diameter funnel-type rainfall cylinder. Immediately after each precipitation event, the precipitation samples were stored in 50 mL HDPE bottles and then placed in a refrigerator at an ambient temperature of 4 °C for cold storage until experimental analysis. The sample measurements were carried out in the stable isotope laboratory of the School of Geography and Environmental Science, Northwest Normal University, with the analytical instrument T-LWIA-45-EP liquid water

isotope analyzer developed by ABB-Los Gatos Research, which has a testing accuracy of ±1‰ for δ^2H and ±0.3‰ for δ^{18}O. In order to avoid memory effects from interfering with the test results during the analysis, each precipitation sample was repeated six times, the first two test results were deleted, and the arithmetic mean of the last four test results was used to represent the isotopic composition of the sample. The results of the analysis are expressed as the difference in thousandths relative to V-SMOW. Precipitation isotope values for a given period are calculated as a weighted average based on the amount of precipitation and are calculated as follows:

$$\delta = \frac{\sum \delta_i P_i}{\sum P_i} \tag{1}$$

where δ is the weighted average of isotopes; δ_i is the isotopic value of a single sample; P_i is the corresponding precipitation amount.

In addition, precipitation vapor isotope data are calculated from the corresponding precipitation isotope data [22], and the calculation formula is as follows:

$$\delta^{18}\mathrm{O}_{PV} = \delta^{18}\mathrm{O}_P - 10^3\left(\alpha^{18}_{W-V} - 1\right) \tag{2}$$

$$\delta^{2}\mathrm{H}_{PV} = \delta^{2}\mathrm{H}_P - 10^3\left(\alpha^{2}_{W-V} - 1\right) \tag{3}$$

where the subscripts PV and P represent precipitation water vapor and precipitation, respectively; $\alpha^{18}{}_{W\text{-}V}$ and $\alpha^{2}{}_{W\text{-}V}$ represent the equilibrium fractionation coefficients of oxygen and hydrogen isotopes, respectively, which have the following relationship with temperature T (K) [22]:

$$10^3 \ln \alpha^{18}_{W-V} = 1.137(10^6/T^2) - 0.4156(10^3/T) - 2.0667 \tag{4}$$

$$10^3 \ln \alpha^{2}_{W-V} = 24.844(10^6/T^2) - 76.248(10^3/T) + 52.612 \tag{5}$$

2.3. Meteorological Data and Reanalysis Data

In this study, the meteorological data were mainly obtained from the daily value dataset of Chinese ground climate data (V3.0) and the hourly observations of China's ground meteorological stations, both of which were provided by the China Meteorological Science Data Center (http://data.cma.cn); the data used for back trajectory simulations were obtained from the National Centers for Environmental Prediction (NCEP) Global Data Assimilation System (GDAS ftp://arlftp.arlhq.noaa.gov/pub/archives/gdas1) with a spatial resolution of 1° × 1°; and water vapor transport heights were calculated by the Laplace pressure equation [35]:

$$H_{cb} = 18400\left(\frac{1 + T_{mean}}{273}\right)\lg\frac{P}{P_{LCL}} \tag{6}$$

where T_{mean} is the average air temperature (°C) of condensation height (LCL) and surface, P is the air pressure at the sampling point (hPa), and P_{LCL} is the air pressure at LCL, calculated as follows [36]:

$$P_{LCL} = P\left(\frac{T_{LCL}}{T}\right)^{3.5} \tag{7}$$

where T_{LCL} and T are the condensation height and the air temperature at the sampling point (K), respectively, and T_{LCL} is calculated as follows:

$$T_{LCL} = T_d - (0.001296T_d + 0.1963)(T - T_d) \tag{8}$$

where T_d is the dew point temperature at the sampling point (°C), T is the sampling point air temperature (°C)

The raindrop diameter was calculated using the following equation [19]:

$$D_{50} = \sqrt[n]{0.69} A I^P \tag{9}$$

where D is the diameter of raindrops (mm), I is the intensity of precipitation (mm/h), and the parameters n, A and P are taken as 2.25, 1.30 and 0.232, respectively.

2.4. Backward Trajectory Model and Specific Humidity Correction

The water vapor transport trajectory of each precipitation event in this study is simulated by the HYSPLIT model, which has been widely used for moisture source studies [21–23]. In this study, the location parameters are the latitude, longitude, and altitude of the sampling point; the starting time is based on hourly observations from ground-based weather stations in China, which are converted to UTC time and input into the model; and the water vapor transport height is calculated by the Laplace pressure equation. Considering that the average residence time of water vapor in the atmosphere does not exceed 10 days [37], the duration is first set to 240 h, and then the specific humidity is corrected. The principle of the specific humidity correction is specifically that the source site of water vapor is judged when the specific humidity at an earlier moment (with an interval of 6 h) is higher than the specific humidity at a later moment by more than 0.2 g/kg and the simulated altitude of the air mass trajectory lies below the planetary boundary layer during the water vapor trajectory retracing process. For the multiple source locations calculated, the location with the largest sum of successive increases in specific humidity and successive changes in specific humidity is used as the source location of water vapor. If the specific humidity on the backward trajectory is less than 0.05 g/kg, it is considered that there is no more water vapor recharge before and is not retraced [21,23,38]. In addition, the backward trajectories were clustered in meteoinfo software in an angular way.

2.5. Potential Source Contribution Factor Analysis

The PSCF (Potential Source Contribution Factor) analysis is commonly applied in air pollution studies [39,40], and is a method to identify potential pollution source areas based on conditional probability functions. Many recent studies have demonstrated the high feasibility of PSCF analysis in the field of moisture source studies [22,30]. In this study, isotopes are embedded into the PSCF analysis as a way to identify potential evaporation source areas. The principle is that when all trajectories are passing through a certain area, the value of a certain element (water vapor *d-excess* value) corresponding to its arrival at the sampling point exceeds a set threshold (average value of water vapor *d-excess*). The water vapor *d-excess* value of the trajectory is considered high and the evaporation of the subsurface corresponding to this grid is strong, which is a potential evaporation source area for the study point. When the grid is far from the study point, the n_{ij} decreases, making the error of PSCF analysis increase and the uncertainty increase. To control this uncertainty, W_{ij} (weight function) is multiplied by the PCSF value [41], and the determination of the weight function is referred to in the literature [42,43]. The calculation formula is as follows:

$$\mathrm{PSCF}_{ij} = \frac{m_{ij}}{n_{ij}} \tag{10}$$

$$\mathrm{WPSCF} = W_{ij} \times \mathrm{PSCF} \tag{11}$$

$$W_{ij} \begin{cases} 1.00 \; 80 < n_{ij} \\ 0.70 \; 20 < n_{ij} \leq 80 \\ 0.42 \; 10 < n_{ij} \leq 20 \\ 0.05 \; n_{ij} \leq 10 \end{cases} \tag{12}$$

where n_{ij} is the total number of trajectories in the grid cells of the selected study area, and m_{ij} is the number of trajectories where the water vapor *d-excess* exceeds its threshold.

3. Results and Discussion

3.1. Preliminary Analysis of the Seasonal Distribution of Precipitation Isotopes

A total of 188 precipitation samples were collected during the observation period. The variation of δ^{18}O ranged from −21.35‰ to 3.10‰, with a weighted average value of −9.14‰; the variation of δ^{2}H ranged from −166.33‰ to 35.71‰, with a weighted average value of −60.16‰; and the variation of *d-excess* ranged from −19.44‰ to 31.16‰, with a weighted mean of 12.97‰ (Figure 3). Comparing the samples collected in the summer half-year and the winter half-year, a total of 115 precipitation samples were collected in the summer half-year, the variation range of δ^{18}O was −21.35‰ to 3.10‰, and the weighted average was −8.13‰; the variation range of δ^{2}H was -166.33‰~35.71‰, the weighted average is −53.42‰; the variation range of *d-excess* is −19.44‰~27.99‰, and the weighted average is 11.61‰. A total of 73 precipitation samples were collected in the winter half-year, and the variation range of δ^{18}O is −21.33‰~−1.45‰, the weighted average is −12.29‰; the variation range of δ^{2}H is −151.89‰~3.62‰, the weighted average is −81.19‰; the variation range of *d-excess* is −7.80‰~31.16‰, and the weighted average is 17.20‰. The maximum and minimum values of δ^{18}O and δ^{2}H are from the samples in the summer half-year. Two features can be observed through the above statistical analysis: (1) precipitation isotopes have obvious seasonal variations, with higher precipitation δ^{18}O and δ^{2}H values in the summer half-year and lower values in the winter half-year, while *d-excess* is lower in the summer half-year and higher in the winter half-year, and similar results have been observed in the surrounding areas [44,45]; (2) precipitation δ^{18}O and δ^{2}H have a greater fluctuation range in the summer half-year compared to the winter half-year, which may be related to the more complex source of water vapor in the summer half-year.

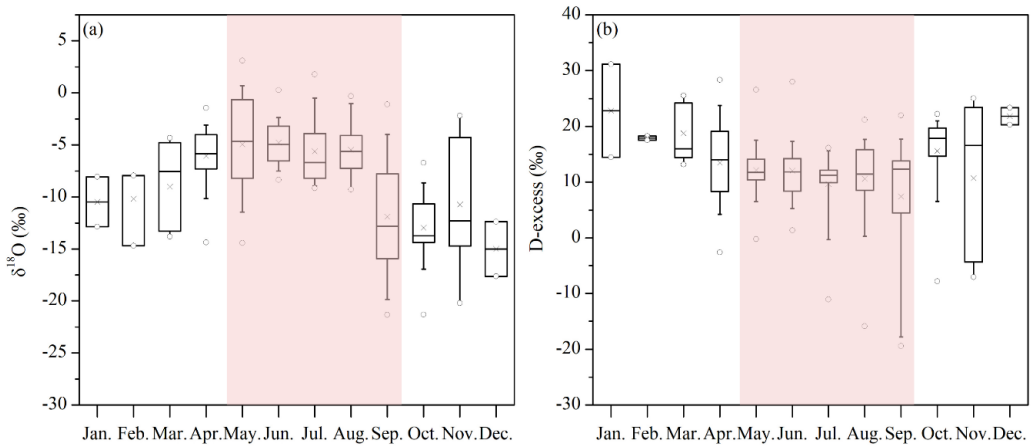

Figure 3. Box line plots of δ^{18}O (**a**) and *d-excess* (**b**) in event precipitation for the 12 months from April 2019 to October 2021, where the shaded area is the summer half; the top and bottom of the box are the 25th and 75th percentiles, the whiskers are maxima and minima, the line near the middle of the box is the median, the cross is the mean, and the hollow circles are the outliers.

3.2. Preliminary Analysis of the Influence of Meteorological Parameters on Precipitation Isotopes

Figure 4 shows the relationship between precipitation δ^{18}O and each local meteorological parameter (temperature, precipitation, and relative humidity). It can be seen from Figure 4 that temperature has the most significant effect on precipitation isotopes, and temperature shows a positive correlation with precipitation δ^{18}O, with a linear regression equation of $\delta^{18}\text{O} = 0.40T–11.79$ ($R^2 = 0.17$; $p < 0.01$). The effect of relative humidity on precipitation δ^{18}O was the next most significant, with a linear regression equation of $\delta^{18}\text{O} = -0.21RH + 9.42$ ($R^2 = 0.13$; $p < 0.01$). The precipitation effect was less pronounced, with precipitation δ^{18}O showing a weak negative correlation with precipitation, with a linear regression equation of $\delta^{18}\text{O} = -0.14P–7.24$ ($R^2 = 0.03$, $p < 0.05$), which is consistent with the results of previous studies in the surrounding area [44–46]. Previous studies have shown that when $P < 5$ mm or RH < 90%, strong subcloud evaporation would make the

temperature effect of precipitation δ^{18}O more pronounced and would weaken the relationship between precipitation δ^{18}O and precipitation amount [22]. Considering that the precipitation samples with $P < 5$ mm (or RH < 90%) accounted for more than 60% of the total number of samples in this study, this may be one of the reasons for the obvious temperature effect. However, the correlation coefficients (r) between precipitation δ^{18}O and T, RH, and P are all less than 0.5, which, together with the reference to previous studies [47,48], suggests that other factors would have more important effects on precipitation isotopes.

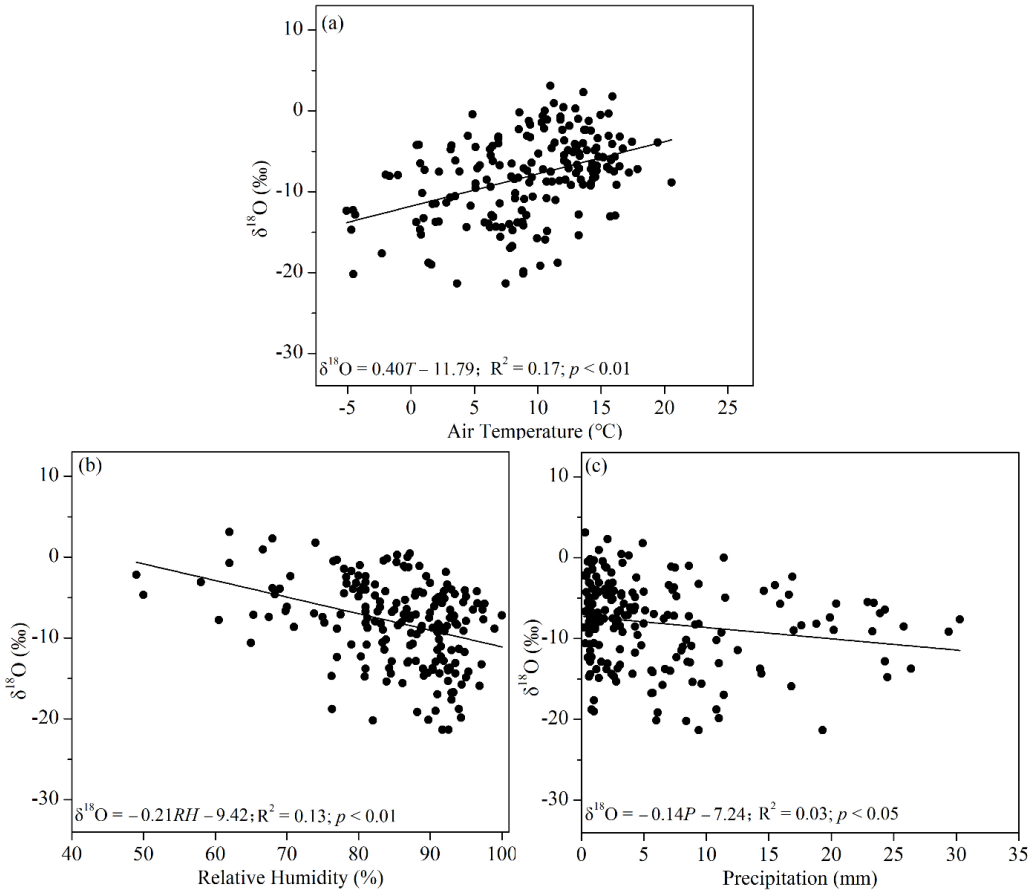

Figure 4. Correlations between δ^{18}O and air temperature (T), precipitation amount (P), and relative humidity (RH).

3.3. Effects of Moisture Sources on Precipitation Isotopes

The model has been widely used in geographic studies, and its simulation results can clearly indicate the moisture source and the water vapor transport trajectory. However, most previous studies have not considered this effect when applying this model to simulations, and the simulation time is set to a constant value, which makes the simulation results uncertain. This uncertainty can be reduced by performing a specific humidity correction of the simulation results according to the method described in Section 2.2, which has been applied in several studies [21,23,38].

Figure 5 shows the water vapor transport trajectories before and after the specific humidity correction for each precipitation event at the sampling site, and the trajectories are significantly shorter after the specific humidity correction. According to the backward trajectory before the specific humidity correction, the precipitation vapor at the sampling point is mainly from Central Asia and Siberia, and there is also water vapor from the East China Sea and the South China Sea in the summer half-year. Previous studies have also shown similar results [30,32]. The backward trajectories show different degrees of shortening after the specific humidity correction, the average water vapor transport time in the summer half-year is about 5 days, and the water vapor mainly comes from the middle

and lower reaches of the Yangtze River plain, the Sichuan Basin and northern Xinjiang; the water vapor transport time in the winter half-year takes about 3.5 days on average, and the water vapor mainly comes from Xinjiang and Inner Mongolia. From this point of view, it is very necessary to correct the specific humidity of the backward trajectory, and uniformly using the same backtracking time for the trace of the moisture source may obtain unrealistic results.

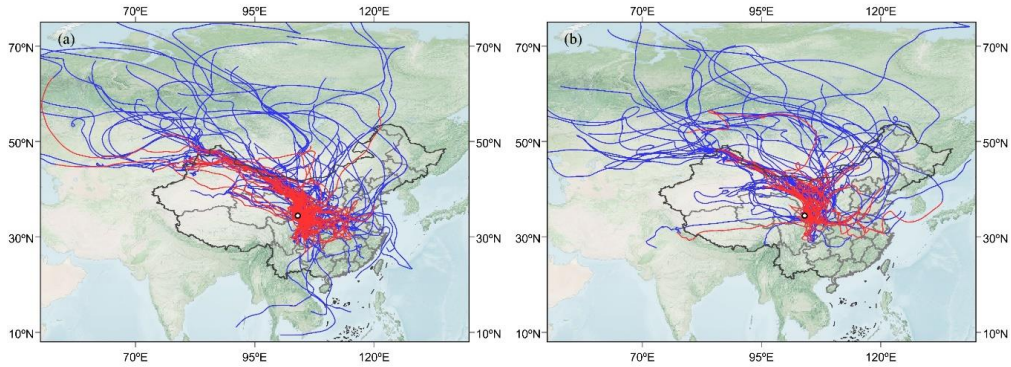

Figure 5. The water vapor transport trajectories of Minxian Station in the summer half-year (**a**) and winter half-year (**b**), the red line is the trajectory after specific humidity correction, and the blue line is the trajectory without specific humidity correction.

3.3.1. Effect of Different Moisture Source Regions on Precipitation Isotopes

The moisture source regions are considered to be an important factor influencing precipitation isotopes [13–16]. Due to the differences in evaporation conditions in different moisture source regions, the resulting precipitation has different isotopic values. *d-excess*, as a secondary variable of precipitation isotopes, can better indicate the information of moisture source area. In general, *d-excess* is negatively correlated with the relative humidity in the moisture source region [17,18].

The clustering of the backward trajectories helps to clarify the main moisture sources, and Figure 6 shows the results of clustering the backward trajectories in the form of angular clustering. From Figure 6, it can be seen that the moisture sources at the sampling sites in the summer half-year are more complex and diverse, and the water vapor is mainly divided into four categories, with water vapor from the northwest and the east as the main sources, whose percentages are 43.48% and 31.30%, respectively, and less water vapor from the northeast and the south, whose percentages are 9.57% and 15.65%, respectively. The water vapor from the sampling sites in the winter half-year can be divided into three categories, with 50.68% from the northwest, 30.14% from the northeast, and 19.18% from the east, and this type of water vapor is mainly concentrated in April and October. Next, the statistical analysis of precipitation due to each type of water vapor was carried out on this basis.

In the summer half-year, the precipitation δ^{18}O caused by NW and S cluster water vapor is relatively close, and its isotopic value is enriched compared with the precipitation caused by NE and E cluster water vapor (Figure 7a), while the corresponding *d-excess* showed unexpected results. Considering the relative humidity of the moisture source area, the *d-excess* of the NW cluster should be the highest one among them, but from Figure 7b, the *d-excess* of the NW cluster is the lowest, and from Figure 7c, the precipitation due to the water vapor of the NW cluster is also the least. This phenomenon is caused by the influence of subcloud evaporation. Since the climate of the sampling site is semi-humid, precipitation in such a climate background will be affected by subcloud evaporation, especially for samples with low precipitation, this effect is more obvious. Subcloud evaporation will lead to the enrichment of precipitation δ^{18}O and *d-excess* decrease, which forms the NW cluster water vapor caused by the most enriched precipitation δ^{18}O and the smallest *d-excess*. For other clusters, the δ^{18}O of the precipitation caused by the water vapor of the S cluster is the highest, specifically $\delta^{18}O_S > \delta^{18}O_E > \delta^{18}O_{NE}$, and it can be seen from Figure 7b that $d\text{-}excess_S$

> *d-excess*$_E$ > *d-excess*$_{NE}$, which better corresponds to the results inferred from the spatial distribution of relative humidity in China [49]. The average precipitation due to these three clusters of water vapor is above 8.5 mm (Figure 7c), in which case the precipitation isotopes are little affected by subcloud evaporation. Therefore, it appears that water vapor transported from the south may result in precipitation with more enriched isotope values. The water vapor in the winter half-year can be divided into three clusters, among which the precipitation δ^{18}O caused by the E cluster water vapor is the most enriched and the *d-excess* is the smallest (Figure 7d, e). The specific performance of the precipitation δ^{18}O caused by the three clusters of water vapor is $\delta^{18}O_E > \delta^{18}O_{NW} > \delta 18O_{NE}$, the *d-excess* performance is *d-excess*$_{NW}$ > *d-excess*$_{NE}$ > *d-excess*$_E$, the three clusters precipitation due to water vapor, and the average precipitation is below 4.5 mm (Figure 7f). Although the temperature is below 0 °C for most of the winter half-year and the subcloud evaporation effect of precipitation isotopes is not obvious, the E cluster water vapor is mainly concentrated in April and October in the winter half of the year and precipitation δ^{18}O is still affected by subcloud evaporation in these two months, so precipitation caused by E cluster water vapor is the most enriched in δ^{18}O and the lowest in *d-excess*.

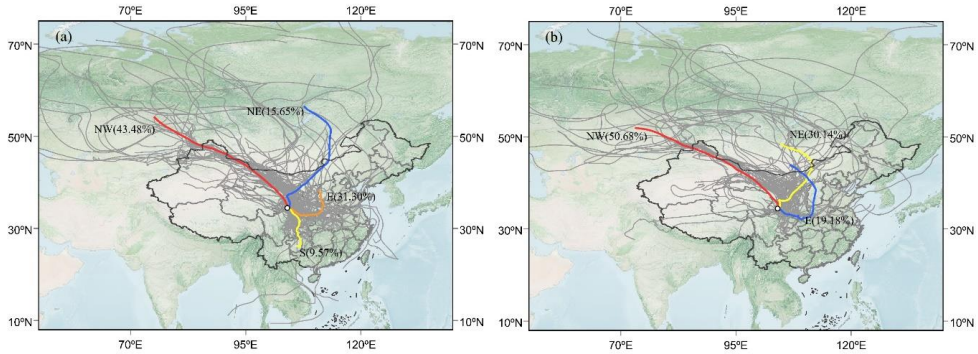

Figure 6. Cluster analysis of water sources in Minxian Station in the summer half-year (**a**) and winter half-year (**b**), the colored lines are the clustering results, and the gray lines are the water vapor trajectory.

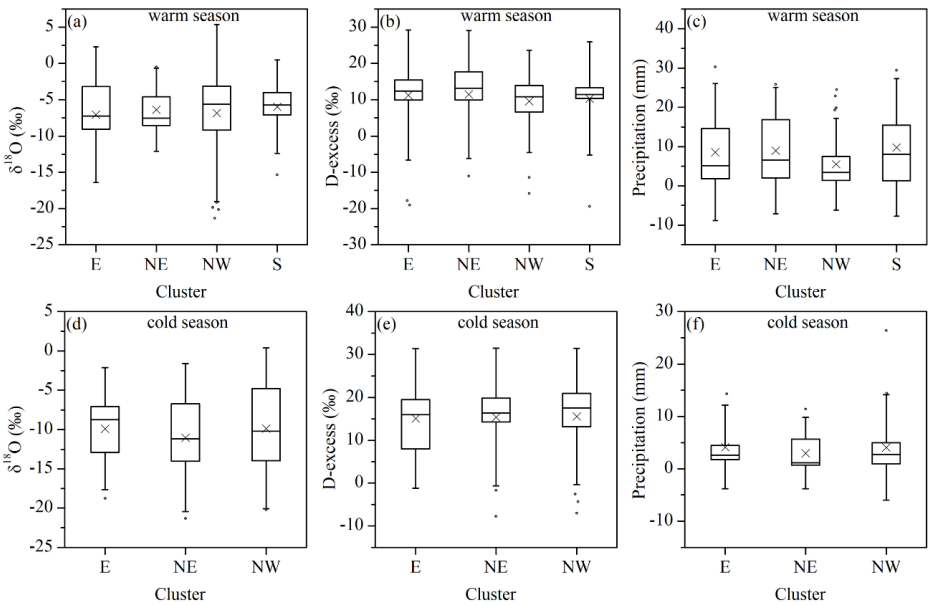

Figure 7. Box line plots of δ^{18}O, *d-excess*, and precipitation for each cluster of water vapor in Minxian Station in the summer half-year (**a**–**c**) and winter half-year (**d**–**f**), the top and bottom of the box are the 25th and the 75th percentile, the line near the middle of the box is the median, the intersection is the mean, the black dots are outliers, and the whiskers are the mean plus or minus 2 standard deviations.

3.3.2. Effect of Water Vapor Transport Time on Precipitation Isotopes

To assess the effect of water vapor transport time on precipitation isotopes, this section analyzes the relationship between precipitation δ^{18}O and water vapor transport time. Figure 8 shows that the relationship between precipitation δ^{18}O and water vapor transport time is different for different time periods. In the summer half-year, the precipitation δ^{18}O showed a fluctuating decreasing trend with the prolongation of water vapor transport time, and the precipitation δ^{18}O showed a negative correlation with the water vapor transport time (Figure 8a); however, in the winter half-year, with the increase of trajectory retracing days, the precipitation δ^{18}O is in a fluctuating state and did not show a decreasing trend with the prolongation of water vapor transport time (Figure 8b). This may be related to the amount of water vapor in the atmosphere. In the summer half-year, the water vapor content in the atmosphere is at a high level due to strong evaporation, which leads to frequent precipitation events in the summer half-year. In the process of water vapor transportation, with the occurrence of precipitation events, heavy isotopes first fall to the surface with the occurrence of precipitation events, while light isotopes continue to be transported with the migration of air masses, resulting in more and more depleted isotope values in subsequent precipitation. Therefore, the precipitation δ^{18}O shows a decreasing trend with the prolongation of the water vapor transport time in the summer half-year, and a similar phenomenon is also observed in other regions [50,51]. In the winter half-year, the water vapor content in the air is at a low level, and precipitation events rarely occur during the water vapor transport, so this trend is not obvious in the winter half-year.

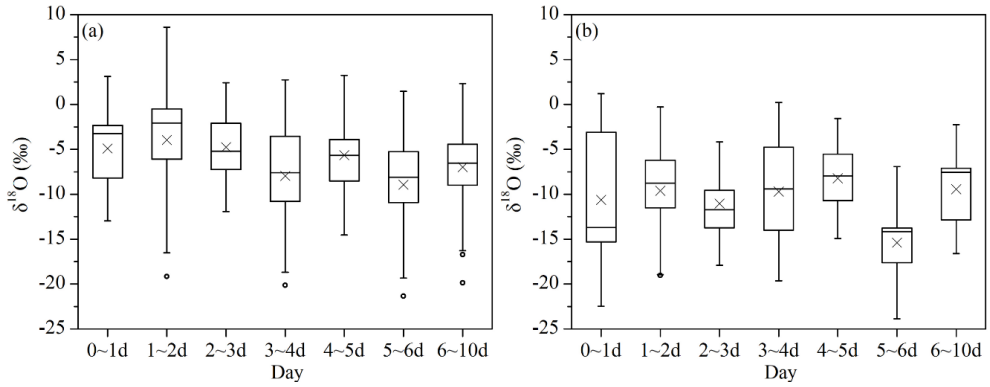

Figure 8. The relationship between the backward trajectory backtracking time and δ^{18}O in precipitation at Minxian Station in the summer half-year (**a**) and winter half-year (**b**), the top and bottom of the box are the 25th and 75th percentiles, and the line near the middle of the box is the median, the cross is the mean, the black dots are outliers, and the whiskers are the mean plus or minus 2 standard deviations.

3.3.3. Effect of Water Vapor Transport Height on Precipitation Isotopes

Since the climate of the study area is semi-humid, subcloud evaporation can have an important effect on precipitation isotopes. In general, the higher the cloud base, the more intense the evaporation to which the raindrops are subjected during their descent, and the higher the corresponding precipitation isotope values [20,49]. As shown in Table 1, precipitation δ^{18}O and cloud base height show a positive correlation in both the winter and summer half-year. It is noteworthy that the positive correlation between precipitation δ^{18}O and cloud bottom height is stronger in the winter half-year compared to the summer half-year. However, by comparing the three most important meteorological factors (cloud bottom height, relative humidity, and temperature) affecting the subcloud evaporation effect under clouds and combining them with previous studies (Table 1), it can be seen that the positive correlation between precipitation δ^{18}O and cloud bottom height should be stronger in the summer half-year. This is obviously not consistent with the results of this study. There are two explanations for this: (1) as shown in Table 1, the raindrop diameters are larger in the summer half-year compared to the winter half-year, and the

smaller raindrops are more susceptible to evaporation during their descent; and (2) the relatively complex moisture source in the summer months may weaken the relationship between precipitation δ^{18}O and cloud bottom height.

Table 1. Correlation coefficient between precipitation δ^{18}O and cloud bottom height and related meteorological parameters.

Correlation Coefficient and Related Meteorological Parameters	Summer Half-Year	Winter Half-Year
Correlation coefficient (all precipitation)	0.45 **	0.49 **
Correlation coefficient ($P \leq 5$mm)	0.29 *	0.42 **
Correlation coefficient ($P \leq 3$mm)	0.32 *	0.43 *
Average cloud bottom height/m	520.80	421.25
Average relative humidity/%	84.66	86.34
Average temperature/°C	12.35	4.43
Average raindrop diameter/mm	1.14	1.00

Note: "**" Statistically significant at the 0.01; "*" Statistically significant at the 0.05.

3.4. Influence of Local Recycled Vapor on Precipitation Isotopes

Water vapor produced by surface evaporation and plant transpiration, collectively referred to as local recycled vapor, is an important component of precipitation vapor. Numerous scholars have previously investigated the contribution of local recycled vapor to precipitation using two-component mixing models and three-component mixing models that incorporate isotope techniques [26–29]. Although these models can better estimate the contribution of local recycled vapor to precipitation, they cannot present the spatial distribution of potential evaporation source areas.

The PSCF analysis combined with the isotope technique can solve this problem well. Figure 9 presents the potential evaporation source areas in the study area in the winter half-year and summer half-year, and it is obvious that the potential evaporation source areas in the summer half-year are more extensive than those in the winter half-year. In the summer half-year, the potential evaporation source areas are mainly distributed in the northern, eastern and southern area of the sampling sites, specifically in the southeastern part of Gansu Province, the eastern part of Sichuan Province and the southern part of Shaanxi Province. In the winter half-year, the potential evaporation source areas are mainly distributed in the southeastern part of Gansu Province and the southern part of Shaanxi Province. This may be the reason for the large range of precipitation isotope fluctuations in the summer half-year. In addition, the results of the PSCF model analysis are overlaid with the backward trajectory after the specific humidity correction to further assess the contribution of local recycled vapor to precipitation (Figure 10). Specifically, if the end of the backward trajectory is within the potential evaporation source areas, it is considered as local recirculating water vapor; if the end of the backward trajectory is outside the potential evaporation source areas, it is considered as advection transported water vapor. The contribution of local recycled vapor to precipitation was calculated to be approximately 32.17% in the summer half-year (Figure 10a) and 24.66% in the winter half-year (Figure 10b), which is more similar to the results of studies using the three-component mixing model in surrounding locations [31]. Since the temperature is below 0 °C for most of the winter half-year, the local recycled vapor in the winter half-year was further investigated. As seen in Figure S1, the spatial distribution of potential evaporation source areas in April and October is similar to that in the winter half-year, while there are almost no potential evaporation source areas in November–March of the year. On this basis, the contribution of local recycled vapor to precipitation in April and October was further calculated, and the result is 22.64% (Figure S2), which is very close to the result in the winter half-year. This indicates that despite the low temperatures in the winter half-year, surface evaporation and transpiration of plants are weak, but local recycled vapor still exists in the winter half-year due to the high temperatures in April and October.

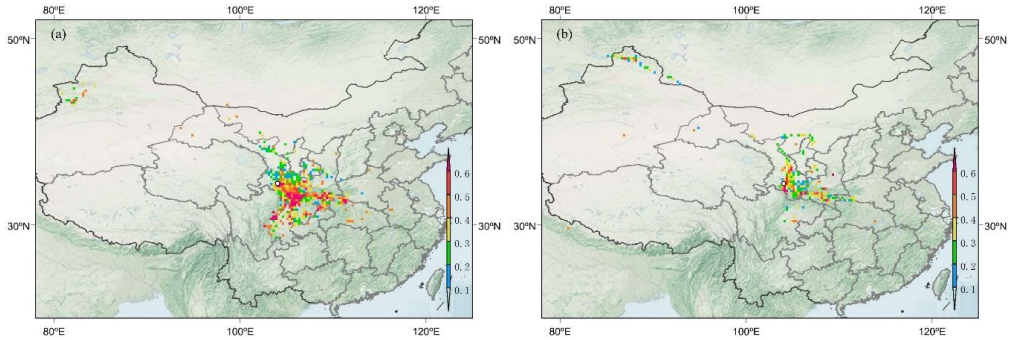

Figure 9. The potential evaporation source area of Minxian Station in the summer half-year (**a**) and winter half-year (**b**).

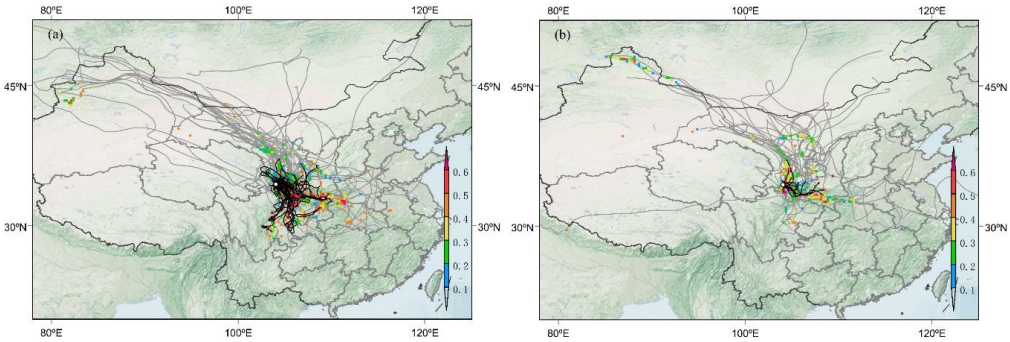

Figure 10. Advective transport of water vapor (grey) and local recycled vapor (black) in the summer half-year (**a**) and winter half-year (**b**) of Minxian Station.

4. Conclusions

In this paper, we used the precipitation samples collected at Minxian Station from 2019 to 2021 to analyze the influence of moisture source on precipitation isotopes, and used PSCF analysis to evaluate the contribution of local recycled vapor to precipitation. The analysis found that precipitation δ^{18}O has obvious seasonal changes, precipitation δ^{18}O was enriched in the summer half-year but depleted in the winter half-year, and precipitation δ^{18}O had a larger fluctuation range in the summer half-year. Among many local meteorological factors, temperature has the most significant impact on precipitation isotopes, but since the correlation coefficient (r) is less than 0.5, this indicates that other factors in the precipitation process have more important effects on precipitation isotopes.

The HYSPLIT model was used to simulate the water vapor transport trajectory, and the specific humidity correction was performed. The results suggest that Xinjiang and the middle and lower reaches of the Yangtze River may be the main moisture sources, rather than Central Asia and the East China Sea, as previously thought. This shows that the specific humidity correction of the backward trajectory is very meaningful. On this basis, the effects of moisture sources, water vapor transport time, and water vapor transport height on precipitation isotopes are further analyzed. In the summer half-year, water vapor from the northwest and the south leads to isotopically enriched precipitation, water vapor from the northeast and the east leads to isotopically depleted precipitation, and water vapor from the northwest leads to precipitation with higher isotopic values, mainly due to subcloud evaporation. In the winter half-year, water vapor from the west and the northeast leads to isotopically depleted precipitation, while water vapor from the east leads to isotopically enriched precipitation, which is also influenced by subcloud evaporation. The time of water vapor transport is another important factor. In the summer half-year, the precipitation δ^{18}O shows a tendency of depletion with the prolongation of water vapor transport time, but this tendency is not obvious in the winter half-year, which may be related to the lower water vapor content in the winter half-year. The effect of water vapor

transport height should not be neglected either. The relationship between precipitation $\delta^{18}O$ and water vapor transport height is positive in both the summer half-year and winter half-year, but this relationship is stronger in the winter half-year, which may be related to the smaller raindrop diameter in the winter half-year and the more complex moisture source in the summer half-year.

The potential evaporation source areas at the sampling sites were clarified using PSCF analysis, which compensated for the inability of previous studies to clarify the spatial distribution of the areas generating local recycled vapor. The study showed that the range of potential evaporation source areas in the summer half-year was larger and mainly distributed in the eastern and southern part of the sampling area, while the range of potential evaporation source areas in the winter half-year was smaller. In addition, the contribution of local recycled vapor to precipitation was evaluated by overlaying the potential evaporation source area and the backward trajectory corrected for specific humidity for analysis, which was 32.17% in the summer half-year and 24.66% in the winter half-year. This study will improve our understanding of the influence of moisture sources on precipitation isotopes and provide a reference for the study of water cycle processes and ecological protection in the western part of the Loess Plateau.

Supplementary Materials: The following are available online at https://www.mdpi.com/article/10.3390/w14213452/s1, Figure S1: Potential evaporation source areas at Minxian Station in October and April (a) and from November to March (b), Figure S2: Advective transported water vapor (grey) and locally recirculated water vapor (black) in October and April (a) and from November to March (b) at Minxian Station.

Author Contributions: Conceptualization, M.Z.; Software, X.Y.; Validation, X.Y.; Formal analysis, X.Y.; Investigation, X.Y.; Methodology, M.Z., D.Q. and S.W; Resources, M.Z., D.Q.and F.C; Data curation, F.C., Y.Z. and Y.T.; Writing—original draft preparation, X.Y.; Writing—review and editing, X.Y., M.Z., D.Q. and S.W.; Supervision, M.Z.; Funding acquisition, M.Z. All authors have read and agreed to the published version of the manuscript.

Funding: The study has financially supported by National Natural Science Foundation of China (42071047).

Data Availability Statement: The data used in this paper are available from M.Z. (mjzhang2004@163.com) upon request.

Acknowledgments: Thank the colleagues of the Northwest Normal University for their help in field work, laboratory analyses, data processing and so on.

Conflicts of Interest: The authors declare no conflict of interest. The work described here has not been submitted elsewhere for publication, in whole or in part, and all the authors listed have approved the manuscript that is enclosed.

References

1. Bowen, G.J.; Cai, Z.Y.; Fiorella, R.P.; Putman, A.L. Isotopes in the water cycle: Regional- to global-scale patterns and applications. *Annu. Rev. Earth Planet. Sci.* **2019**, *47*, 453–479. [CrossRef]
2. Sayemuzzaman, M.; Jha, M.K. Seasonal and annual precipitation time series trend analysis in north carolina, united states. *Atmos. Res.* **2014**, *137*, 183–194. [CrossRef]
3. Klein, E.S.; Nolan, M.; Mcconnell, J.; Sigl, M.; Cherry, J.; Young, J.; Welker, J.M. Mccall glacier record of arctic climate change: Interpreting a northern alaska ice core with regional water isotopes. *Quat. Sci. Rev.* **2016**, *131*, 274–284. [CrossRef]
4. Hu, J.; Julien, E.-G.; Tabor, C.; Nusbaumer, J.; Partin, J. Deciphering oxygen isotope records from chinese speleothems with an isotope-enabled climate model. *Paleoceanogr. Paleoclimatol.* **2019**, *34*, 2098–2112. [CrossRef]
5. Gui, J.; Li, Z.X.; Feng, Q.; Yuan, R.F.; Ning, T.T.; Zhang, B.J.; Xue, J.; Gao, W.D.; Nan, F.S.; Ding, W.X.; et al. Environmental effect and spatiotemporal pattern of stable isotopes in precipitation on the transition zone between the Tibetan Plateau and arid region. *Sci. Total Environ.* **2022**, *605*, 127350. [CrossRef]
6. IPCC. Climate change 2021—The physical science basis. *Chem. Int.* **2021**, *43*, 22–23. [CrossRef]
7. Wang, T.; Chen, J.S. Long-term trend of precipitation stable isotopic compositions under global warming conditions. *J. Radioanal. Nucl. Chem.* **2020**, *325*, 557–565. [CrossRef]
8. Zheng, J.; Fan, J.L.; Zhang, F.C. Spatiotemporal trends of temperature and precipitation extremes across contrasting climatic zones of china during 1956–2015. *Theor. Appl. Climatol.* **2019**, *138*, 1877–1897. [CrossRef]

9. Dansgaard, W. Stable isotopes in precipitation. *Tellus* **1964**, *16*, 436–468. [CrossRef]
10. Yao, T.D.; Masson-Delmotte, V.; Gao, J.; Yu, W.S.; Yang, X.X.; Risi, C.; Sturm, C.; Werner, M.; Zhao, H.B.; He, Y.; et al. A review of climatic controls on δ^{18}O in precipitation over the Tibetan Plateau: Observations and simulations. *Rev. Geophys.* **2013**, *51*, 525–548. [CrossRef]
11. Xia, C.C.; Liu, G.D.; Mei, J.; Meng, Y.C.; Liu, W.; Hu, Y. Characteristics of hydrogen and oxygen stable isotopes in precipitation and the environmental controls in tropical monsoon climatic zone. *Int. J. Hydrog. Energy* **2019**, *44*, 5417–5427. [CrossRef]
12. Gou, J.F.; Qu, S.M.; Guan, H.D.; Shi, P.; Su, Z.G.; Lin, Z.H.; Liu, J.T.; Zhu, J. Relationship between precipitation isotopic compositions and synoptic atmospheric circulation patterns in the lower reach of the Yangtze River. *J. Hydrol.* **2022**, *605*, 127289. [CrossRef]
13. Tian, L.D.; Yao, T.D.; MacClune, K.; White, J.W.C.; Schilla, A.; Vaughn, B.; Vachon, R.; Ichiyanagi, K. Stable isotopic variations in west China: A consideration of moisture sources. *J. Geophys. Res. Atmos.* **2007**, *112*, 380. [CrossRef]
14. Wei, R.; Tian, L.D.; Shao, L.L. Regional moisture sources and Indian summer monsoon (ISM) moisture transport from simultaneous monitoring of precipitation isotopes on the southeastern and northeastern Tibetan Plateau. *J. Hydrol.* **2021**, *601*, 126836. [CrossRef]
15. Wu, S.Y.; Bedaso, Z. Quantifying the effect of moisture source and transport on the precipitation isotopic variations in northwest Ethiopian Highland. *J. Hydrol.* **2022**, *605*, 127322. [CrossRef]
16. Yu, W.S.; Wei, F.L.; Ma, Y.M.; Liu, W.J.; Zhang, Y.Y.; Luo, L.; Tian, L.D.; Xu, B.Q.; Qu, D.M. Stable isotope variations in precipitation over deqin on the southeastern margin of the Tibetan Plateau during different seasons related to various meteorological factors and moisture sources. *Atmos. Res.* **2016**, *170*, 123–130. [CrossRef]
17. Guan, H.D.; Zhang, X.P.; Skrzypek, G.; Sun, Z.A.; Xu, X. Deuterium excess variations of rainfall events in a coastal area of South Australia and its relationship with synoptic weather systems and atmospheric moisture sources. *J. Geophys. Res. Atmos.* **2013**, *118*, 1123–1138. [CrossRef]
18. Uemura, R.; Matsui, Y.; Yoshimura, K.; Motoyama, H.; Yoshida, N. Evidence of deuterium excess in water vapor as an indicator of ocean surface conditions. *J. Geophys. Res. Atmos.* **2008**, *113*, 210. [CrossRef]
19. Wang, S.J.; Zhang, M.J.; Che, Y.J.; Zhu, X.F.; Liu, X.M. Influence of below-cloud evaporation on deuterium excess in precipitation of arid central Asia and its meteorological controls. *J. Hydrometeorol.* **2016**, *17*, 1973–1984. [CrossRef]
20. Kong, Y.L.; Pang, Z.H. A positive altitude gradient of isotopes in the precipitation over the Tianshan Mountains: Effects of moisture recycling and sub-cloud evaporation. *J. Hydrol.* **2016**, *542*, 222–230. [CrossRef]
21. Crawford, J.; Hughes, C.E.; Parkes, S.D. Is the isotopic composition of event based precipitation driven by moisture source or synoptic scale weather in the Sydney Basin, Australia? *J. Hydrol.* **2013**, *507*, 213–226. [CrossRef]
22. Shi, Y.D.; Wang, S.J.; Wang, L.W.; Zhang, M.J.; Argiriou, A.A.; Song, Y.; Lei, S.J. Isotopic evidence in modern precipitation for the westerly meridional movement in Central Asia. *Atmos. Res.* **2021**, *259*, 105698. [CrossRef]
23. Wang, S.J.; Zhang, M.J.; Crawford, J.; Hughes, C.E.; Du, M.X.; Liu, X.M. The effect of moisture source and synoptic conditions on precipitation isotopes in arid central Asia. *J. Geophys. Res. Atmos.* **2017**, *122*, 2667–2682. [CrossRef]
24. Van der Ent, R.J.; Savenije, H.H.; Schaefli, B.; Steele-Dunne, S.C. Origin and fate of atmospheric moisture over continents. *Water Resour. Res.* **2010**, *46*, 449. [CrossRef]
25. Gao, Y.H.; Chen, F.; Miguez-Macho, G.; Li, X. Understanding precipitation recycling over the Tibetan Plateau using tracer analysis with WRF. *Clim. Dyn.* **2020**, *55*, 2921–2937. [CrossRef]
26. Wang, S.J.; Zhang, M.J.; Che, Y.J.; Chen, F.L.; Qiang, F. Contribution of recycled moisture to precipitation in oases of arid central Asia: A stable isotope approach. *Water Resour. Res.* **2016**, *52*, 3246–3257. [CrossRef]
27. Kong, Y.L.; Pang, Z.H.; Froehlich, K. Quantifying recycled moisture fraction in precipitation of an arid region using deuterium excess. *Tellus B Chem. Phys. Meteorol.* **2013**, *65*, 19251. [CrossRef]
28. Zhang, Z.X.; Zhu, G.F.; Pan, H.X.; Sun, Z.G.; Sang, L.Y.; Liu, Y.W. Quantifying recycled moisture in precipitation in Qilian Mountains. *Sustainability* **2021**, *13*, 12943. [CrossRef]
29. Chen, F.L.; Zhang, M.J.; Wu, X.X.; Wang, S.J.; Argiriou, A.A.; Zhou, X.; Chen, J.F. A Stable Isotope Approach for Estimating the Contribution of Recycled Moisture to Precipitation in Lanzhou City, China. *Water* **2021**, *13*, 1783. [CrossRef]
30. Wu, X.X.; Chen, F.L.; Liu, X.Y.; Wang, S.J.; Zhang, M.J.; Zhu, G.F.; Zhou, X.; Chen, J.F. The Significance of Hydrogen and Oxygen Stable Isotopes in the Water Vapor Source in Dingxi Area. *Water* **2021**, *13*, 2374. [CrossRef]
31. Li, X.F.; Lu, A.G.; Feng, Q.; Li, Z.; Liu, W.G.; Wang, S.J.; Tripathee, L.; Wang, X.Y.; Cao, J.J. Recycled moisture in an enclosed basin, Guanzhong Basin of Northern China, in the summer: Contribution to precipitation based on a stable isotope approach. *Environ. Sci. Pollut. Res.* **2020**, *27*, 27926–27936. [CrossRef] [PubMed]
32. Chen, F.L.; Zhang, M.J.; Ma, Q.; Wang, S.J.; Li, X.Y.; Zhu, X.F. Stable isotopic characteristics of precipitation in Lanzhou City and its surrounding areas, Northwest China. *Environ. Earth Sci.* **2015**, *73*, 4671–4680. [CrossRef]
33. Sun, C.J.; Chen, W.; Chen, Y.N.; Cai, Z.Y. Stable isotopes of atmospheric precipitation and its environmental drivers in the Eastern Chinese Loess Plateau, China. *J. Hydrol.* **2020**, *581*, 124404. [CrossRef]
34. Cai, Z.Y.; Tian, L.D.; Bowen, G.J. ENSO variability reflected in precipitation oxygen isotopes across the Asian Summer Monsoon region. *Earth Planet. Sci. Lett.* **2017**, *475*, 25–33. [CrossRef]
35. Berberan-Santos, M.N.; Bodunov, E.N.; Pogliani, L. On the barometric formula. *Am. J. Phys.* **1997**, *65*, 404–412. [CrossRef]
36. Barnes, S.L. An empirical shortcut to the calculation of temperature and pressure at the lifted condensation level. *J. Appl. Meteorol. Climatol.* **1968**, *7*, 511. [CrossRef]

37. Yang, K.; Koike, T.; Fujii, H.; Tamura, T.; Xu, X.; Bian, L.; Zhou, M. The daytime evolution of the atmospheric boundary layer and convection over the Tibetan Plateau: Observations and simulations. *J. Meteorol. Soc. Japan. Ser. II* **2004**, *82*, 1777–1792. [CrossRef]
38. Sodemann, H.; Schwierz, C.; Wernli, H. Interannual variability of Greenland winter precipitation sources: Lagrangian moisture diagnostic and North Atlantic Oscillation influence. *J. Geophys. Res. Atmos.* **2008**, *113*, 256. [CrossRef]
39. Jiang, H.M.; Li, Z.Q.; Zhang, X.; Wang, F.T.; Zhou, X.; Wang, F.L.; Zhang, Y.F.; Zheng, C.Y.; Song, M.Y.; Chen, T.T. Chemical components characteristics and source analysis of $PM_{2.5}$ over Lanzhou city in winter and summer. *J. Environ. Sci.* **2021**, *41*, 1690–1702. [CrossRef]
40. Wang, R.; Ding, J.L.; Ma, W.; Zhang, J.Y.; Han, L.J. Analysis of atmospheric particulates source in Urumqi based on PSCF and CWT model. *J. Environ. Sci.* **2021**, *41*, 3033–3042. [CrossRef]
41. Xu, X.; Akhtar, U.S. Identification of potential regional sources of atmospheric total gaseous mercury in Windsor, Ontario, Canada using hybrid receptor modeling. *Atmos. Chem. Phys.* **2010**, *10*, 7073–7083. [CrossRef]
42. Zeng, Y.; Hopke, P.K. A study of the sources of acid precipitation in Ontario, Canada. *Atmos. Environ.* **1989**, *23*, 1499–1509. [CrossRef]
43. Meng, H.F.; Zhang, M.J.; Wang, S.J.; Qiu, X.; Du, M.X.; Zhang, Y.N.; Yu, X.X.; Zhou, S.E. Isotopic characteristics of water vapor and its sources during day and night along the Heihe River in summer. *Arid. Lang Geogr.* **2020**, *43*, 360–370.
44. Wan, H.; Liu, W.G.; Xing, M. Isotopic composition of atmospheric precipitation and its tracing significance in the Laohequ Basin, Loess plateau, China. *Sci. Total Environ.* **2018**, *640*, 989–996. [CrossRef] [PubMed]
45. Chen, F.L.; Zhang, M.J.; Wang, S.J.; Qiu, X.; Du, M.X. Environmental controls on stable isotopes of precipitation in Lanzhou, China: An enhanced network at city scale. *Sci. Total Environ.* **2017**, *609*, 1013–1022. [CrossRef]
46. Li, Z.X.; Feng, Q.; Song, Y.; Wang, Q.J.; Jiao, Y.; Li, Y.G.; Li, J.G.; Cuo, X.Y. Stable isotope composition of precipitation in the south and north slopes of Wushaoling Mountain, northwestern China. *Atmos. Res.* **2016**, *182*, 87–101. [CrossRef]
47. Wang, D.; Tian, L.D.; Cai, Z.Y.; Shao, L.L.; Guo, X.Y.; Tian, R.; Li, L.K.; Chen, Y.L.; Yuan, C. Indian monsoon precipitation isotopes linked with high level cloud cover at local and regional scales. *Earth Planet. Sci. Lett.* **2020**, *529*, 115837. [CrossRef]
48. Gao, J.; Masson-Delmotte, V.; Risi, C.; He, Y.; Yao, T.D. What controls precipitation $\delta^{18}O$ in the southern Tibetan Plateau at seasonal and intra-seasonal scales? A case study at Lhasa and Nyalam. *Tellus B Chem. Phys. Meteorol.* **2013**, *65*, 21043. [CrossRef]
49. Wang, S.J.; Jiao, R.; Zhang, M.J.; Crawford, J.; Hughes, C.E.; Chen, F.L. Changes in below-cloud evaporation affect precipitation isotopes during five decades of warming across China. *J. Geophys. Res. Atmos.* **2021**, *126*, e2020JD033075. [CrossRef]
50. Yu, W.S.; Yao, T.D.; Tian, L.D.; Ma, Y.; Wen, R.; Devkota, L.P.; Wang, W.C.; Qu, D.M.; Chhetri, T.B. Short-term variability in the dates of the Indian monsoon onset and retreat on the southern and northern slopes of the central Himalayas as determined by precipitation stable isotopes. *Clim. Dyn.* **2016**, *47*, 159–172. [CrossRef]
51. Guo, X.Y.; Tian, L.D.; Wen, R.; Yu, W.S.; Qu, D.M. Controls of precipitation $\delta^{18}O$ on the northwestern Tibetan Plateau: A case study at Ngari station. *Atmos. Res.* **2017**, *189*, 141–151. [CrossRef]